

Seeking simplicity for the understanding of multiphase flows

Howard A. Stone

*Department of Mechanical and Aerospace Engineering, Princeton University,
Princeton, New Jersey 08544, USA*

(Received 2 July 2017; published 17 October 2017)

Fluid mechanics is a discipline with rich phenomena, with motions occurring over an enormous range of length scales, and spanning a wide range of laminar and turbulent flows, instabilities, and applications in industry, nature, biology, and medicine. The subfield of complex fluids typically refers to those flows where the complexity is introduced, for example, by the presence of suspended particles, multiple phases, soft boundaries, and electrokinetic effects; several distinct multiphase flows of Newtonian fluids make up the examples in this article. Interfaces play a significant role and modify the flow with feedback that further changes the shapes of the interfaces. I will provide examples of our work highlighting (i) new features of classical instabilities triggered by changes in geometry, (ii) multiphase flows relevant to the design of liquid-infused substrates exhibiting effective slip while retaining the trapped liquid, and (iii) unexpected dynamics in flow at a T-junction. The interplay of experiments and mathematical models and/or simulations is critical to the new understanding developed.

DOI: [10.1103/PhysRevFluids.2.100507](https://doi.org/10.1103/PhysRevFluids.2.100507)

I. INTRODUCTION

A. Beauty and surprises in fluid dynamics

All scientists and researchers like to think that their subject is more captivating and interesting than the topics studied by others. We should all be so inspired to want to study and learn about the many corners of our chosen field of intellectual inquiry. Nevertheless, one feature that characterizes fluid dynamics is the breadth of subject areas to which the ideas apply: from geophysical studies of oceans, atmospheres, and planetary interiors, which occur on length scales of thousands of kilometers for Earth, to problems of swimming and flying, which occur on scales from fractions of a meter to tens of meters (e.g. birds, fish, airplanes, satellites), to medical devices, which operate at the scales of millimeters to fractions of a meter, and down to the scale of the cell (typically microns to tens of microns) and micro- and nano-fluidic devices. This range from thousands of kilometers to smaller than microns thus introduces challenges over more than 12 orders of magnitude in length scale, and the subjects include practically every science and engineering department at a university. Of course, this intellectual breadth often makes it challenging for fluid dynamicists from different disciplines to talk with one another!

A further distinguishing feature of fluid dynamics is that the flows often make for beautiful pictures and videos. Some of this beauty is captured every year by the Gallery of Fluid Motion at the Annual Meeting of the Division of Fluid Dynamics (DFD) of the American Physical Society. An early recognition of the role of visualization for understanding fluid motions was the impetus for Milton van Dyke's unique book *An Album of Fluid Motion* [1], which still plays an important role in our education as a supplement to classroom discussions and lectures; a modern variant of this book is now available that draws on many contributions to the Gallery of Fluid Motion [2]. If a reader seeks inspiration, then these collections of still images are a great starting point (and videos from the annual gallery at the 2016 DFD meeting are available at <https://gfm.aps.org/>).

As one elegant example of fluid dynamics in nature, which is certain to be of interest to scientist and lay person alike, consider phalaropes, which are shore birds that have an unusual approach to meals. Typically, they feed by spinning in circles as illustrated in Fig. 1, which displays still images of the clockwise movements of a phalarope as it pecks at the surface [Fig. 1(a)], as well as the motion

HOWARD A. STONE

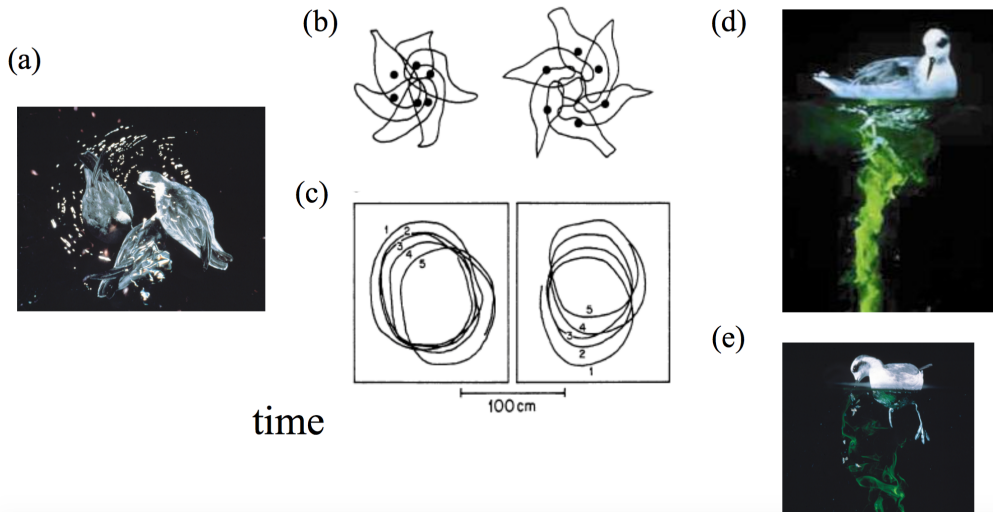


FIG. 1. Fluid dynamics and phalaropes. (a) A multiexposure image of a phalarope in three separate positions as it spins. (b) A single spin of a phalarope with the body outlined. (c) Motion of the centroid of two phalaropes during multiple spins. (d) Flow patterns imaged with fluorescein dye placed in a dish in the water below the phalarope. (e) A phalarope feeding on a meal worm while spinning. Panels (b)–(d) are from Ref. [3], the images in (a) and (c) were extracted by W. Hamner from a video he took, and the photos in (d) and (e) were taken by National Geographic photographer Bates Littlehales (deceased). (b–d) Reprinted by permission from Macmillan Publishers Ltd: *Nature (London)* **384**, 121, copyright 1996. I thank W. Hamner for sharing photos of the phalarope’s dynamics and information about their origin.

of a bird’s centroid [Figs. 1(b) and 1(c)] that highlights the circular motion [3]. This feeding strategy succeeds because the circular movements produce a vortex, which is documented in Fig. 1(d), where fluorescein dye is added to water; the vortex generates an up-flow, bringing food up to the surface from the water below and so the phalarope enjoys its meal. The opening and closing of the shore bird’s beak involves a surface-tension–induced transport of water drops that contain prey [4], which is another fluid dynamics problem. It is tempting to ask what other fluid dynamics problems the phalarope has solved!

B. A spectrum of challenges with complex fluids and multiphase flows

It is worth contrasting the very different ways that complexity can enter fluid mechanics problems. At one end of the spectrum are single-phase, incompressible high-Reynolds-number turbulent flows, which mathematically derive their complexity (and mystery) from the coupled nonlinear partial differential equations that are the continuity and Navier-Stokes equations. Of course, there are reacting or multiphase high-Reynolds-number flows, but not surprisingly they only add to the complexity of an already complicated problem.

At the other end of the spectrum are low-Reynolds-number flows, where often the inertia terms in the equations of motion are negligible and the fluid flow is typically laminar (and it is common to think about the flow as simple), but the complexity comes through the need to understand a dynamically evolving interface or suspended particles, which feed back to alter the flow. Thus, the subject of “complex fluids” refers to flows where the complexity is introduced by the presence of suspended particles (e.g., cells, polymers) and multiple phases, and includes soft boundaries, electrokinetic effects (flows influenced or driven by the presence of ions in solutions), etc.; several such multiphase flow problems form the examples discussed in this article. These problems naturally link the subject of fluid mechanics to many science and engineering disciplines, and span such

problems as the flows of emulsions and foams [5] as is common in industrial processes, the impact of the rheology of blood in studies of hemodynamics (which also is relevant at higher Reynolds numbers), and the manipulation of particles using chemical gradients (the topic of diffusiophoresis) in small devices [6–9]. With this definition, some problems are naturally very old, such as the effective viscosity of a suspension of spheres, which dates back to Einstein’s pioneering work at the beginning of the 20th century. Related questions now arise in studies of the effective viscosity or the self-organization of an active suspension [10], such as swimming microorganisms or synthetic versions of active particles. As a further example, it is now known that small amounts of polymer in an otherwise Newtonian fluid in a Taylor-Couette flow introduce elastic instabilities [11] even when the Reynolds number is small and the Newtonian solution is stable; when these effects are present in common flow configurations, effectively turbulent velocity fluctuations are triggered, so-called elastic turbulence, again even when the Reynolds number is small [12].

Flow problems involving complex fluids and/or multiphase flows often lead to puzzling initial observations that require a variety of control experiments to identify the dominant or important physical processes at play; typically theory, or more frequently modeling, is needed hand-in-hand with the experiments to obtain qualitative understanding and, hopefully, quantitative descriptions. For example, in recent years I have been fortunate to work with colleagues to study and understand:

(i) How the oscillations of a free surface are damped by the presence of a thin layer of foam [Figs. 2(a)–2(c)] [13]

(ii) How the coalescence cascade, whereby a drop deposited on a bath of the same liquid undergoes a sequence of coalescence and bouncing processes with the drop size progressively decreasing, is modified to a single, rapid collapse process when surfactants, above a critical concentration, are present in the drop [Figs. 2(d)–2(f)] [14]

(iii) How the motion of a bubble in a channel with circular cross section, where the continuous phase is a suspension of small particles, is modified in time as the particles attach to the interface to form an “armored shell,” which in turn influences the thickness and shape of the thin film between the bubble and the wall [Figs. 2(g)–2(h)] [15]

(iv) How the dissolution of CO_2 in a channel flow of water creates a transverse chemical (ion) gradient that, via a process called diffusiophoresis, drives the particles to one side of the channel and so a stream of particle-free water is obtained, which thus suggests “membraneless filtration” [Figs. 2(i)–2(k)] [9]

(iv) How the viscosity variations in a fluid, due to presence of a sphere hotter or colder than the surroundings, causes particle motions that modify typical textbook results in low-Reynolds-number hydrodynamics, including the case of a “Janus” sphere, characterized by a thermal dipole Δ , which couples translation \mathbf{U} and rotation $\mathbf{\Omega}$ of the sphere [Figs. 2(l)–2(m)] [16].

The range of problems studied by the research community is of course much broader. The advances in microfabrication, high-speed imaging, and imaging or microscopy more generally, along with advances in computing and open-source software, including excellent software for solving the Navier-Stokes equations and free-boundary problems, are allowing researchers to tackle ever more complicated problems. Of course, I would like to believe that there is still a role for simplified models that help identify dominant features that control a flow.

To appreciate the possible changes in the dynamics that can occur in the simplest versions of the mechanics of multiphase flows, we note that the presence of an interface introduces the surface tension γ , which represents a force/length or energy/area. When the gravitational acceleration (g) matters, then the ratio of γ to ρg , where ρ is the fluid density, introduces a natural length scale, $\ell_c = (\frac{\gamma}{\rho g})^{1/2}$, which is known as the capillary length. This length scale compared to a natural geometric length scale, e.g., ℓ , defines the Bond number, $\mathcal{B} = \frac{\ell^2}{\ell_c^2}$. Furthermore, dynamical processes with typical speed v in a viscous fluid (viscosity μ) produce stresses that deform interfaces. The ratio of viscous stresses, $\mu v/\ell$ to typical capillary stresses γ/ℓ associated with interfaces curved on the scale ℓ introduce the capillary number $\mathcal{C} = \frac{\mu v}{\gamma}$. Thus, even when flows are laminar and the governing equations are linear, as occurs when the Reynolds number is small, there are two

HOWARD A. STONE

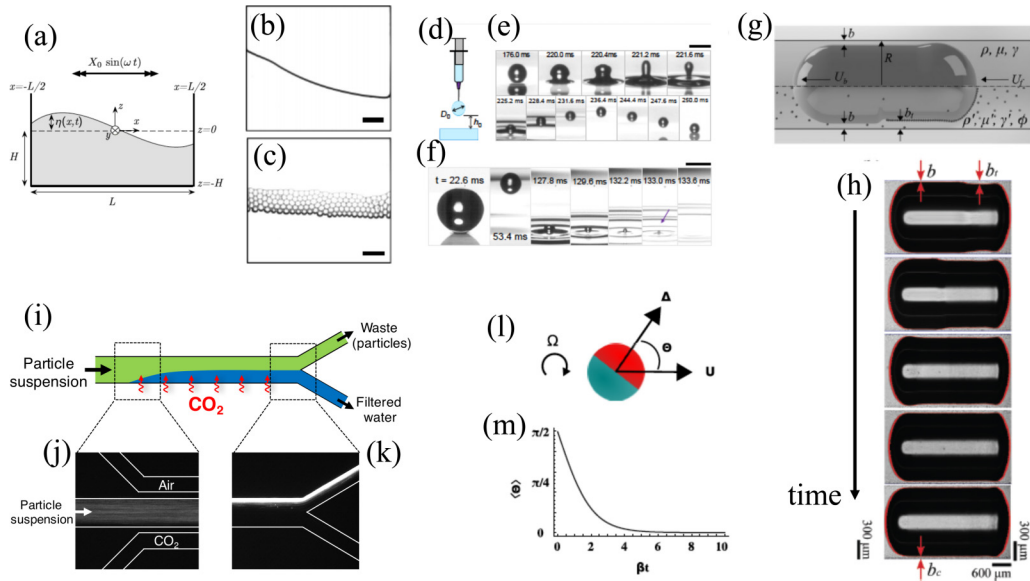


FIG. 2. A variety of problems involving complex fluids and multiphase flows. (a–c) An interface between a liquid and air is perturbed and oscillates; the oscillations are damped by the presence of a thin layer of foam at the interface. Joint work with Alban Sauret, François Boulogne, Jean Cappello, and Emilie Dressaire [13]; reprinted from A. Sauret, F. Boulogne, J. Cappello, E. Dressaire, and H. A. Stone, Damping of liquid sloshing by foams, *Phys. Fluids* **27**, 022103 (2015) with the permission of AIP Publishing. (d–f) The damped coalesce cascade whereby a drop with surfactant coalesces almost immediately with a bath of the same liquid without, in the absence of surfactants, undergoing a previously documented cascade of rebound-coalescence events. The scale bars are 1 mm. Joint work with Suin Shim. Figure reproduced from Ref. [14]. (g–h) Translation of a bubble in a tube with circular cross section, where the continuous phase contains a suspension of small particles; the particles adhere to the liquid-air interface, alter the local film thickness relative to regions with the particle armor, and so modify the speed of the bubble. Joint work with Estella Yu and Sepideh Khodaparast [15]; reproduced from Soft Matter with permission from the Royal Society of Chemistry. (i–k) Diffusiophoresis, which refers to the movement of particles in a chemical gradient, here driven by dissolution of CO_2 into water. The flow is left to right, and the particles migrate to one side of a channel where they can be separated, thus providing a route to “membraneless filtration” of the original solution. Each of the channels has a width about $100 \mu\text{m}$. Figure reproduced from Ref. [9]. Joint work with Sangwoo Shin, Orest Shardt, and Patrick Warren. (l–m) Translation and rotation of a particle in a fluid in a case where the particle modifies the temperature, and so the viscosity, in the neighborhood of the particle. Here we show the case of a “Janus” sphere, characterized by a thermal dipole Δ , which couples translation U , and rotation Ω . Joint work with Naomi Oppenheimer and Shahin Navardi. Figure reproduced from Ref. [16].

dimensionless parameters \mathcal{B} and \mathcal{C} , which can each span a wide range of values depending on the application, that are needed to understand the shapes of fluid-fluid interfaces, and, correspondingly, the interface shape typically has a large affect on the fluid flow. Mathematically we can also expect that the change in the shape of an interface, which impacts the flow and is itself influenced by the flow, introduces nonlinearity into the problem.

Another area of fluid dynamics that brings new ideas is associated with the advances in microfabrication. In this case, one can consider flows over surfaces with topography. This topic has a small literature in part because of the significant complication associated with a complex boundary, which is compounded if the flow is confined to a thin film (e.g., Refs. [17,18]). To illustrate the surprises that can occur, we first remind the reader of a laboratory hydraulic jump, as can be visualized in a kitchen sink when a water jet of sufficiently high speed impacts the smooth

SEEKING SIMPLICITY FOR THE UNDERSTANDING OF ...

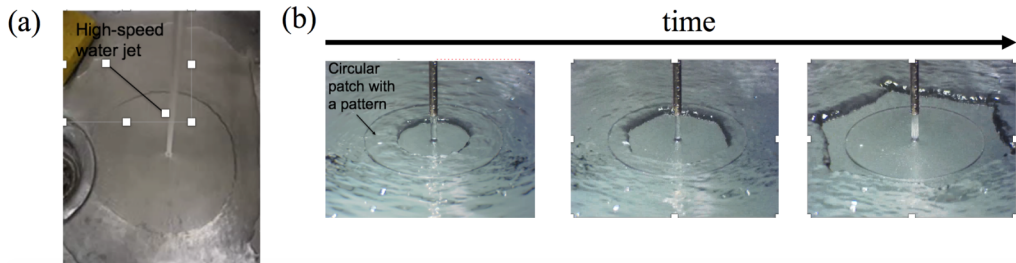


FIG. 3. Hydraulic jumps. (a) A water jet forms a hydraulic jump in a laboratory sink. (b) The hydraulic jump formed by a water jet impacting a surface containing a microfabricated substrate with a hexagonal pattern of circular posts (within the circular patch indicated) outside of which the surface is otherwise smooth. The three images show the response as the flow rate is increased. The flow rate ranges from 0.5 to 2.5 liters/minute and is supplied through a needle of 2 mm diameter. The cylindrical posts have radius $50 \mu\text{m}$ and height $52 \mu\text{m}$. The center-to-center spacing between posts is $200 \mu\text{m}$. The region covered by the posts is a circular disk of radius equal to 2.5 cm (E. Dressaire, personal communication). This problem was studied in Refs. [19,20]. Figure courtesy of E. Dressaire and L. Courbin.

boundary of the sink, as shown in Fig. 3(a). Typically, in these flows the thin film that forms on the substrate has a large Reynolds number but the flow is laminar.

We asked how this flow might change when the substrate contains a micropattern, such as a hexagonal pattern of circular posts where the micro texture was $O(100 \mu\text{m})$ (joint work with E. Dressaire, L. Courbin, and J. Crest). In the experiments we placed a micron-scale pattern within a circular patch that was flush with an otherwise smooth substrate. At low jet speeds the hydraulic jump was nearly circular, but following a step change in flow rate the hydraulic jump increases in radius and takes on an increasing hexagonal shape [Fig. 3(b)], and the jump even exists on the smooth part of the substrate. The dynamics here combine flow within a “porous” microfabricated array of posts with the rapidly flowing thin film above, which brings in the dynamics of the hydraulic jump. This flow was analyzed by allowing for a macroscopic resistance to flow over the substrate, which effectively introduces a heterogeneous friction that reflects the hexagonal micropattern [19,20]. The fact that the hexagonally shaped jump exists outside the region where there is a pattern on the substrate reflects the inertia of the fluid, which is the source of “memory” as the fluid flows over the surface.

This introduction has strived to briefly provide one view of the nature of fluid dynamics problems involving the flow of complex fluids and multiphase flows. The breadth of such problems is vast, and they expose a researcher to a wide range of physics and physical chemistry themes. The dynamics is rich, and often puzzling at first, and so provides a great training ground (in the view of the author) for an education in fluid dynamics, especially with regard to the many applications that often arise across the engineering and science disciplines, including many of relevance in industry.

II. A NEW ANGLE ON THE SAFFMAN-TAYLOR (VISCIOUS FINGERING) INSTABILITY

A. Multiphase flows in small devices

One branch of multiphase flows that has exploded, at least in terms of the number of published papers, if not also in terms of the diversity of ideas and potential applications, is the subject of droplet microfluidics (e.g., Ref. [21]). Most commonly, a two-phase flow is used to make droplets, which themselves are used as chemical containers, or measurement volumes for chemical reactions or the growth of bacteria, or the droplets are solidified by polymerization or chemical reactions; the two phases can also be used to create threads of various aspect ratios, shapes, and compositional complexity (e.g., Ref. [22]). From a theoretical perspective the problems are complicated because of the unknown shape of the fluid-fluid interface, and even numerical solutions are challenging as a

HOWARD A. STONE

consequence of the complicated three-dimensional geometries, the presence of thin films, the need to determine the shape of the free boundary, the possible role of surfactants, etc. In this section, we describe one such flow problem where a new phenomenon was recognized, a simplified model proved useful for understanding the dynamics, and the ideas highlighted a new aspect of a classical instability in fluid dynamics.

B. Historical remarks about viscous fingering

One of the most well-known instabilities in fluid dynamics occurs when a fluid of low viscosity, often air or water, is injected into a fluid of higher viscosity, usually an oil [26]. In the laboratory it is common to perform the experiment between two parallel, rigid, impermeable boundaries, and a common application of the basic ideas is to oil recovery in the porous subsurface of Earth. The two configurations are related mathematically since it is well-known that the average equations for viscously dominated flow between two rigid planes, with depth-averaged velocity $\langle \mathbf{u} \rangle$, are the Darcy equations $\frac{\mu \langle \mathbf{u} \rangle}{k} = -\nabla p + \rho \mathbf{g}$, where k is the permeability, which describe the average motion of a fluid in porous materials. The injection of a fluid might be anticipated to displace the fluid already present in the gap or pores, and this is often the desire so as to remove the “in place” liquid, but reality is different. Instead, the injection of a low-viscosity fluid forms narrow fingers that are the paths of lower resistance, and the injected fluid flows through the system in a finger-like pattern, leaving much of the high viscosity fluid in place.

The viscous fingering phenomenon, generally known as the Saffman-Taylor instability, which derives from a 1958 paper by the named authors [23], had been identified already in the Chemical Engineering literature in 1952 by Hill [24] in a paper including a one-dimensional stability calculation and complementary experiments. The Saffman-Taylor contribution was complemented a short time later by a paper by Chouke *et al.* [25]. After giving a short calculation making clear the potential for instability when the interface is displaced from the less viscous to the more viscous fluid, Saffman and Taylor even commented in their paper that “It appears that this result is not essentially new and that mining engineers and geologists have long been aware of it.” Homsy [26] provides a discussion of these earlier papers in an excellent review of viscous fingering and notes that “the phenomenon under discussion should almost certainly be called the ‘Hill Instability’” in recognition of the pioneering 1952 contribution [26, p. 277].

The viscous fingering phenomenon has been studied in a wide variety of systems, e.g., radial configurations, viscoelastic fluids, etc. To the best of my knowledge prior to the work described next in Sec. II C and II D there was no known stabilizing mechanism for the viscous fingering instability, as it is normally discussed in relation to the work of Saffman and Taylor. We next highlight a role for geometry in altering the traditional stability behavior, and we remark below about the similarity of these ideas to coating flow problems involving thin films on rollers.

C. Experiments on drop breakup by an obstacle

The dynamics that inspired us were experiments performed by Suzie Protière, who investigated the influence of a fixed circular post on droplet motion in a microfluidic channel [27]. A large drop filled the cross section of a channel containing a second immiscible liquid, and as the drop flowed along the channel it encountered a post. Two distinct responses were recorded (Fig. 4). When the drop was more viscous than the surrounding fluid, it was able to deform in such a way that it would pass around the post through only one of the gaps between the post and the channel wall, and the drop did not break. In contrast, when the drop speed was above a critical value, then the drop would flow through both gaps and the drop would break, typically into two unequal volumes.

Extensive experiments convinced us that the key to understanding the dynamics was the motion of the fluid-fluid interface as it passed through the two narrow gaps between the post and the channel walls when the drop encountered the obstacle. The two different cases are illustrated in Fig. 5(a). At sufficiently low speed one meniscus appeared to get slightly ahead, and then all of the drop fluid

SEEKING SIMPLICITY FOR THE UNDERSTANDING OF ...

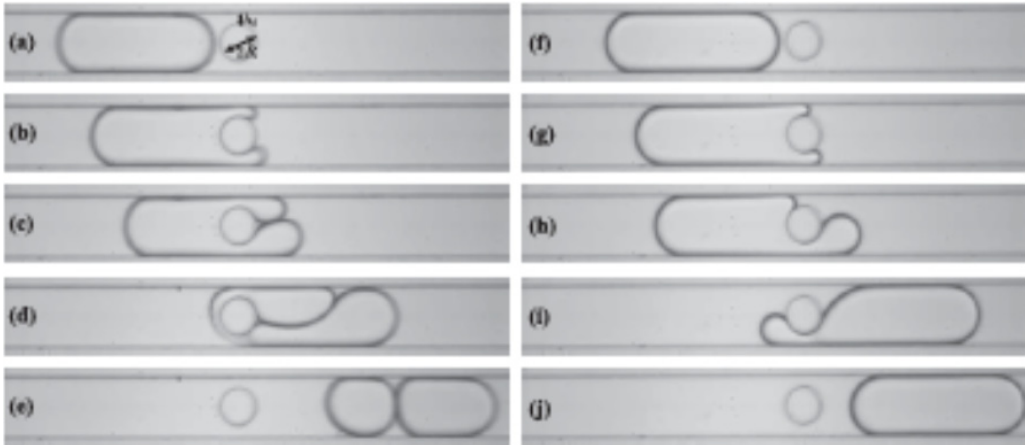


FIG. 4. Experiments in a microfluidic channel of height $w = 50 \mu\text{m}$ (into the page) and width $b = 120 \mu\text{m}$ showing a drop approaching a circular post (radius $R = 40 \mu\text{m}$). The drop is eight times more viscous than the continuous phase. A capillary number is defined as $C = \mu_{\text{drop}} Q / (b w \gamma)$, where Q is the total flow rate of the continuous phase, μ_{drop} is the drop viscosity, and γ is the interfacial tension. Images (a)–(e), $C = 0.06$: (a) $t = 0$ ms, (b) $t = 2.5$ ms, (c) $t = 5$ ms, (d) $t = 11.5$ ms, (e) $t = 17.5$ ms. The drop has broken into two drops downstream of the post. Images (f)–(j), $C = 0.012$: (f) $t = 0$ ms, (g) $t = 20$ ms, (h) $t = 30$ ms. (i) $t = 70$ ms, (j) $t = 82.5$ ms. At this smaller value of the capillary number we observe that the drop does not break up. Figure reproduced from “Droplet breakup in flow past an obstacle: A capillary instability due to permeability variations,” *Europhys. Lett.* **92**, 54002 (2010) [27].

followed. We refer to this case as an instability. When the drop speed was sufficiently fast, both menisci moved nearly together and two drops formed downstream of the post, and we refer to the dynamics of the menisci as stable.

If we simply considered the experiment of Fig. 4 as invasion of one fluid by a second fluid of higher viscosity, and considered the dynamics as a variant of the viscous fingering problem, then there should only be “stability” in the sense used above, as the more viscous fluid should propagate displacing the low-viscosity fluid in front at any interface speed. However, with our focus on the menisci, we noted that because the meniscus had to move through a gap that had a parabolic shape there was necessarily a capillary pressure gradient as the motion occurred and the fluid-fluid interface experienced this gradient of capillary pressure in the flow direction. We then developed a one-dimensional model combining mass conservation and Darcy’s law for the dynamics of two competing menisci (volume conservation links the motion of the two menisci), and the model had the same features as the experiments, as displayed in Fig. 5(b) [27].

These results suggested to us that permeability gradients in the flow direction introduce a feature that had not been previously investigated from the standpoint of altering the familiar viscous fingering phenomenon and which could alter the conventional stability criterion. Nevertheless, we note that there are related problems involving two-phase flows in channels and lubrication geometries that vary in shape along the flow direction, and the influence of capillary effects on the stability of the flow had been recognized [28–32]. For example, in the classic printer’s instability, where the thin films on the surfaces of two closely spaced rotating rollers can experience a transverse or “ribbing” instability, capillary pressure gradients associated with the position of the meniscus control the dynamics.

D. Fluid displacement in a slanted Hele-Shaw cell

In order to better relate the observations of the menisci moving through the parabolically shaped gap in Fig. 4, and to understand the link to the viscous fingering problem, with Talal Al-Housseiny

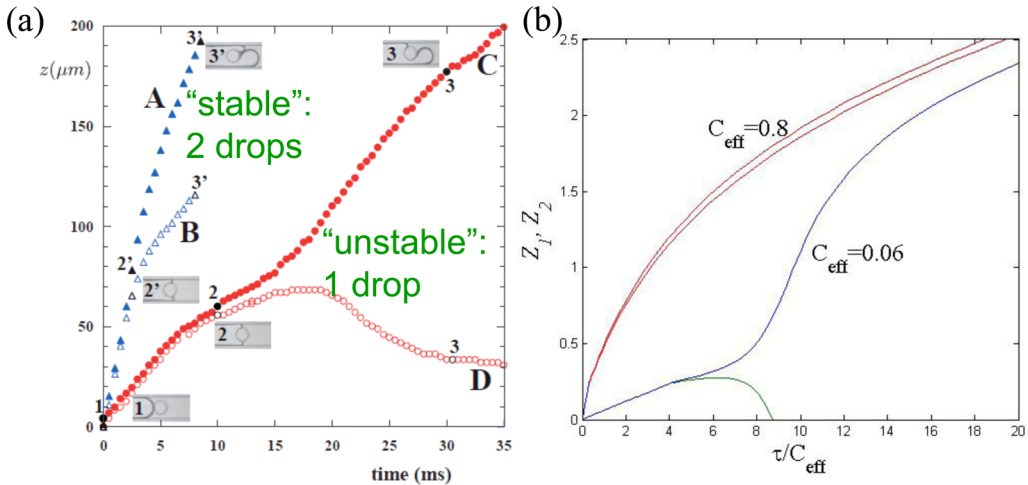


FIG. 5. Position of the menisci as a function of time as a drop encounters an obstacle in a channel (as in Fig. 4) [27]. (a) Experimental results for menisci in the lower (A and C) and upper (B and D) gaps; $\mu_{\text{drop}}/\mu_{\text{cont}} = 8$. $C = 0.06$ for curves A and B, where the drop breaks. $C = 0.012$ for curves C and D, where the drop does not break. Each numbered image shows the position of the menisci. (b) Results of a one-dimensional mathematical model with dimensionless position along the gap Z versus time τ , where C_{eff} is a capillary defined in the model. Figure reproduced from “Droplet breakup in flow past an obstacle: A capillary instability due to permeability variations,” *Europhys. Lett.* **92**, 54002 (2010) [27].

and Amy Tsai we undertook systematic experiments in a Hele-Shaw configuration [33]. In this case, however, we inclined the plates slightly (angle α), which introduces a capillary pressure gradient as a meniscus propagates along the channel. The gradient is not present in the well-studied case of parallel boundaries.

Experimental results pushing water (low viscosity) into silicone oil (high viscosity) with $\alpha < 0$ showed that the displacement process was stable at sufficiently low speeds, or capillary numbers, but that viscous fingers developed above a critical capillary number [Figs. 6(a)–6(d)]. Similarly, if silicone oil (high viscosity) displaced water (low viscosity) with $\alpha < 0$, which traditional ideas would suggest is a stable displacement configuration, we found a critical capillary number below which the flow develops fingers [Figs. 6(e)–6(h)]. Again, the gradient in geometry gives rise to a capillary pressure gradient that causes a change in the stability characteristics of the flow.

The two main fluid parameters are the viscosity ratio λ and a capillary number C and they are now supplemented by a geometric parameter α . We can now anticipate, by analogy with the results in Sec. II C, that there is a critical capillary number C_c for the stability-instability transition and further that the angle of the plates, which sets the capillary pressure gradient (proportional to $\gamma\alpha$), should affect C_c . For a typical flow speed v , the systematic change in shape brings in the ratio of viscous stresses to the change in the capillary stress, i.e., $\mu v/(\gamma\alpha) = C\alpha^{-1}$. A linear stability calculation in the spirit of the classical viscous fingering analysis (e.g., Ref. [26]) leads to the growth rate σ versus wave number k relation (here θ_c is the contact angle, h_0 is a typical gap height, and w is the width) [33] (see also the review of coating flows in Ref. [30] where an analogous result is found):

$$\frac{(1 + \lambda)\sigma}{u_0/w} = \left(1 - \lambda + \frac{2\alpha \cos \theta_c}{C}\right)k - \frac{(h_0/w)^2}{C}k^3. \quad (1)$$

This result involves $C\alpha^{-1}$, which was identified just above by balancing typical viscous and capillary stresses. We note that the growth rate can change sign for some k when

$$1 - \lambda + \frac{2\alpha \cos \theta_c}{C} = 0, \quad (2)$$

SEEKING SIMPLICITY FOR THE UNDERSTANDING OF ...

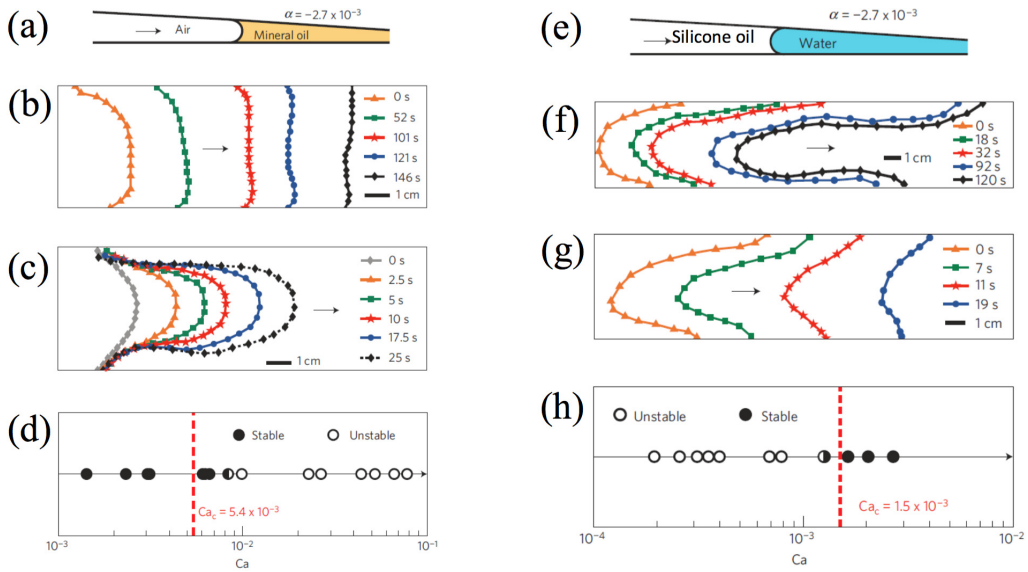


FIG. 6. Inhibiting and triggering viscous fingering in a slanted Hele-Shaw cell. Figure from Ref. [33]. (a) Schematic of the side view of an experiment where air (nonwetting) displaces wetting mineral oil, $\mu_1 = 25 \times 10^{-3}$ kg/m/s. (b) Top view of experiment results where viscous fingering is inhibited at $C = 6 \times 10^{-3}$. (c) Top view of experiment results where the interface is unstable at $C = 1.6 \times 10^{-2}$. (d) Stability diagram for transitions from unstable (open circle) to stable (filled circle) at a critical capillary number C_c , determined experimentally (half-filled circle) and predicted theoretically (red dashes). Note: For this viscosity ratio, the interface is always unstable in a uniform Hele-Shaw cell. (e) Schematic side view of the experimental setup where wetting silicon oil, $\mu_2 = 25 \times 10^{-3}$ kg/m/s, displaces nonwetting water, $\mu_1 = 1 \times 10^{-3}$ kg/m/s. (f) Top view where fingering is triggered $C = 4 \times 10^{-4}$. (g) Top view for $C = 1.6 \times 10^{-3}$ and the system is stable because disturbances decay in time. (h) Stability diagram showing transitions from stable (filled circle) to unstable (open circle) at a critical capillary number C_c , determined experimentally (half-filled circle) and predicted theoretically (red dashes). For this viscosity ratio, the interface is always stable in a uniform Hele-Shaw cell. Figure reproduced from Ref. [33].

which identifies a viscosity-ratio-dependent critical capillary number $C_c = \frac{2\alpha \cos \theta_c}{\lambda - 1}$. This result is consistent, at least qualitatively, with the experimental results shown above and highlights that there is a critical speed or capillary number, dependent on α (geometry), for the transition from stable to unstable displacements. As one other example, this physical idea of the role of a gradient of capillary pressure impacting viscous fingering can be important in fluid displacement in a Hele-Shaw cell with an elastic boundary (e.g., Refs. [34,35]).

III. RETENTION VERSUS FAILURE OF LIQUID-INFUSED SURFACES

In recent years it has become appreciated that making materials that expose a flow to a substrate with an interdigitated set of liquid and solid boundaries offers the potential for an effective slip boundary condition [36–39]. Such an interface can promote the sliding of drops along the surface, which is advantageous for self-cleaning surfaces. The surfaces, as they can contain a liquid with a chemistry different than the solid, have been shown also to be effective for minimizing icing and adhesion of biomaterials.

A. An effective slip length

The presence of a fluid-solid boundary suggests decreased drag when the surface is adjacent to a laminar or turbulent flow. Indeed, there is a large body of recent literature on this topic,

HOWARD A. STONE

including many numerical simulations, all of which implicitly assume that the fluid-solid boundary is retained in the presence of the flow and which report some measure of an “effective slip boundary condition.” I note that Eric Lauga and I reported in 2003 a theoretical study for the effective slip length (a macroscopic characterization of a channel flow) for flow over surfaces with regions of slip imbedded in a no-slip surface [40]; see also Ref. [41]. Our results highlighted the idea that in channel flows the typical laboratory measurements that might suggest slip, e.g., pressure drop versus flow rate measurements, are really probing macroscopic features, not the microscopic details of a local slip length. In particular, a small fraction of a no-slip surface on an otherwise perfect slip boundary has a significant effect in reducing the effective slip length of the macroscopic flow.

In the Lauga-Stone paper we referenced two papers from 1972 by J. R. Philip, who had originally posed similar boundary-value problems for flow past surfaces with periodic distributions of no-slip and perfect slip boundaries, such as those studied in our paper [42,43]. As I recall, I found these papers by accident while browsing research journals in a library, which I suppose happens only rarely now. Amusingly, in the 30 years prior to 2003, Philip’s two papers had been cited only five times and one time, respectively, while in a little more than the 10 years since we brought these nice results to the attention of the fluid dynamics community, Philip’s papers have been cited more than 140 times and 70 times, respectively. Of course, one reason for this fact is the relatively recent interest in near-surface fluid dynamics because of the ability to fabricate and image at the submicron scale.

B. Flow over liquid-infused surfaces

In recent years my research group tackled the question of whether or not such liquid-infused surfaces can retain the liquid when exposed to a shear stress. Thus, we chose to study how these materials might fail when exposed to flow, and if so what design strategies might be invoked to retain the fluid. Jason Wexler and Ian Jacobi led this work, developed the experimental setup illustrated in Fig. 7, and reported experiments and a first mathematical model for understanding our results [44]. In particular, one side of a channel contains many long narrow grooves, typically about 10 microns \times 10 microns in cross section [Fig. 7(d)]. These grooves are filled with a fluid of one viscosity and are then exposed to a channel flow. The flow tends to drain the trapped immiscible fluid until a steady state configuration is established whereby a length L_∞ of liquid is retained in the grooves [Fig. 7(c)].

In the notation commonly adopted in the literature, the fluid in the groove has viscosity μ and the external phase has viscosity $\mu_{\text{ext}} = N\mu$, where the viscosity ratio N is one dimensionless parameter. We worked in conditions of low Reynolds numbers and for the flow rate in the channel Q , which is a natural control variable, we observed that for any N , the retention length $L_\infty \propto Q^{-1}$ [Fig. 8(a) [45]]. Effectively the applied shear stress τ_∞ acting on the interface, which is proportional to Q for a viscously dominated flow, drags trapped liquid along the length of the channel (the pressure gradient along the channel also plays a role), and for these viscous flows, all the data collapse with $L_\infty \propto \tau_\infty^{-1}$ [Fig. 8(b)] and the prefactor is a function of N and ratios of geometric parameters that describe the channel cross section. The interface between the two liquids is curved, and so a capillary pressure gradient is established in the trapped liquid and generates a back flow, which maintains some trapped liquid; a quasisteady state is established balancing capillary effects (proportional to the surface tension γ) with the applied stresses, i.e., $L_\infty \propto \gamma/\tau_\infty$. In further work with Ying Liu and Clarissa Schonecker, we developed a detailed model to rationalize our measurements for all N [45] [Fig. 8(c)].

Our results allow us to develop design strategies for retaining the trapped lubricant in a liquid-infused substrate, at least if a maximum surface shear stress can be estimated. My Princeton colleagues Marcus Hultmark and Lex Smits have been applying these ideas in turbulent channel flows, where the Reynolds numbers are obviously much larger, but the local near-surface flow is characterized by the (turbulent) shear stress.

SEEKING SIMPLICITY FOR THE UNDERSTANDING OF ...

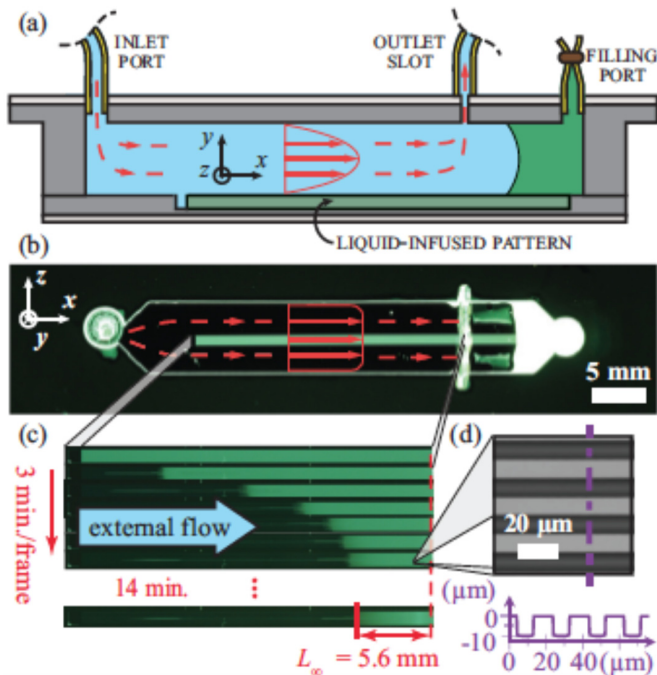


FIG. 7. Experiments with flow over a liquid-infused substrate. (a) Cross section of the microfluidic channel. One fluid fills the main channel, and a second immiscible fluid fills the grooves on one side. (b) Planform view showing the device before drainage begins. Here the 50 longitudinal grooves at the center of the device fluoresce green. (c) Snapshots of a shear-driven drainage experiment subject to an aqueous flow rate $Q = 2$ ml/min. (d) Micrograph of the micropattern used to mold the grooves, which appear dark gray while walls appear light gray. Figure reproduced from Ref. [44].

IV. VORTEX BREAKDOWN AND FLOWS IN COMMON T-JUNCTIONS

As a final example of a “complex” flow, I describe single-phase and multiphase studies we have performed in recent years in a common engineering configuration of a T-junction [see Fig. 9(a)] and other simply branched junctions at other angles. This geometry is typical of a wide range of fluid distribution systems. In particular, for a channel with cross-sectional dimension ℓ , average flow speed $\langle u \rangle$, density ρ and viscosity μ , our interest is in high-Reynolds-number laminar flows, typically $\mathcal{R}_e < 1000$, where $\mathcal{R}_e = \frac{\rho \langle u \rangle \ell}{\mu}$. It is natural for a reader to expect that this flow is well studied, both numerically and experimentally, and well understood. As I will now explain, the former is true and the latter is false, at least as far as I have been able to learn for the range of Reynolds numbers and the flow details that have been the focus of our work.

To describe how we (joint work with Daniele Vigolo and Stefan Radl) stumbled on this problem, I show in Fig. 9(b) experimental observations of the flow of bubbles (in a water flow) through a T-junction when $\mathcal{R}_e = 980$ [46]. Naturally, one expects that the flow should transport the bubbles through the T-junction. To our surprise bubbles get trapped in the junction and accumulate. Gravity does not matter, but the density difference between the bubbles and the liquid is important. We have found no reference in the literature to this phenomenon and in fact now understand it as primarily (for a low number density of bubbles) controlled by a single-phase flow phenomenon, and bifurcation, in this channel configuration.

From three-dimensional numerical simulations of a single-phase flow at comparable Reynolds numbers we were able to understand structural features of the flow and systematic changes to the flow as the Reynolds number is increased. The flow structures are surprising and help us rationalize

HOWARD A. STONE

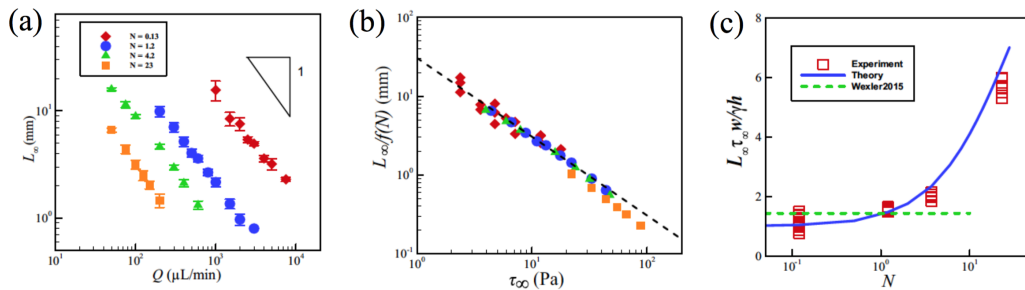


FIG. 8. Measurements of the retention length as a function of the control parameters for flow over liquid-infused surfaces (as in Fig. 7). Figure from Ref. [45]. (a) Retention length L_∞ versus channel flow rate Q for different viscosity ratios N (viscosity of the external phase, μ_{ext} , relative to viscosity of the trapped lubricant). (b) Rescaled steady-state length L_∞ , normalized by a function of N and geometric parameters (see [45]) as a function of the shear stress τ_∞ , where $\tau_\infty = \frac{6\mu_{\text{ext}}Q}{WH^2}$ and W and H are, respectively, the width and height of the main channel. The symbols are defined as in (a). (c) Normalized steady-state length $L_\infty \tau_\infty w / (\gamma h)$, where w and h are, respectively, the width and height of the grooves, as a function of N . The solid and dashed curves are models described by Ref. [45]. Figure reproduced from Ref. [45].

our experimental observations. To illustrate these features we show in Fig. 10 results obtained with Kevin Chen and Clancy Rowley that highlight the appearance of internal stagnation points as the Reynolds number increases [47], as recognized also by Ref. [46]. Above a critical Reynolds number, which is about 300 for the T-junction, and is approximately independent of the radius of curvature of the corners (e.g., see Fig. 2 in Ref. [47]), the flow develops internal circulation zones that are responsible for trapping of low-density objects, such as the bubbles in Fig. 9(b).

It is well known that when inertia matters, such as occurs at finite Reynolds numbers, flow around a bend as in Fig. 9(a), similar to flow in a gently curved pipe (first studied by Dean [48]), involves streamlines that have approximately helical paths and streamwise vorticity. There is axial vorticity and the streamlines throughout the flow begin and end at infinity. When the swirl speed is sufficiently fast relative to the axial flow speed, it is also known in simpler geometries that internal stagnation points can appear so that there are regions of closed streamlines; a bifurcation occurs in the flow. This

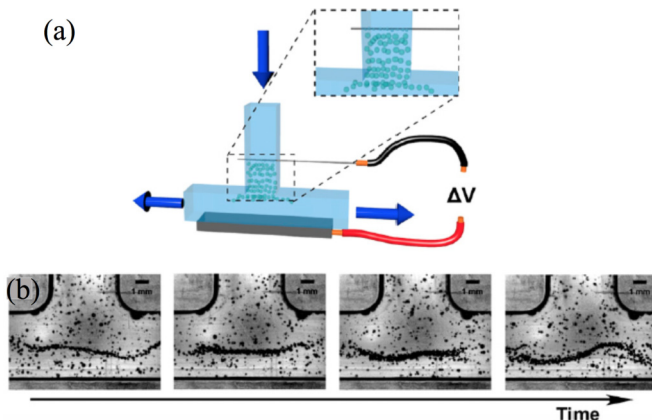


FIG. 9. Flow in a T-junction, with flow entering at the top and leaving out both sides (approximately symmetrically), where small air bubbles appear black. (a) A schematic of our use of electrolysis to generate bubbles in the flow. (b) A time sequence, with images taken every $125 \mu\text{s}$, of the bubbly flow showing bubble trapping during flow of water in a T-junction; lateral size $L = 4.8 \text{ mm}$, $\mathcal{R}_e = 980$. Figure reproduced from Ref. [46].

SEEKING SIMPLICITY FOR THE UNDERSTANDING OF ...

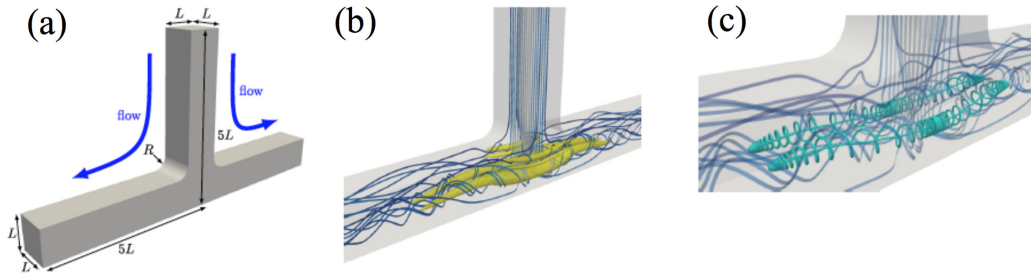


FIG. 10. Vortex breakdown in a T-junction. (a) A numerical study of flow in a T-junction geometry. (b) Streamlines of the flow where color indicates speed (white is high and black is low) for $\mathcal{R}_c = 560$, with radius of curvature of the corners $R = 0.4L$. Yellow illustrates regions of significant vorticity as determined by the Q criterion. (c) For the conditions of (b), the streamlines illustrate the four recirculation regions (cyan), which indicate stagnation points in the flow so that there are effectively regions of closed streamlines. Figure reproduced from Ref. [47]. Reprinted from K. K. Chen, C. W. Rowley, and H. A. Stone, Vortex dynamics in a pipe T-junction: Recirculation and sensitivity, *Phys. Fluids* **27**, 034107 (2015), with the permission of AIP Publishing.

phenomenon is known as vortex breakdown, which has its own somewhat specialized, and indeed apparently somewhat controversial, literature, e.g., ideas based on reorientation of vortex lines [49] versus subcritical to supercritical transitions of inertial waves [50–52]. Given the geometry, the Reynolds number is sufficient to characterize both the flow as the mean flow speed varies and the bifurcation in the flow structure where vortex breakdown occurs.

In work continued by Jesse Ault, Francois Gallaire, and Andrea Fani we have argued, as first suggested by Ref. [46], that the vortex breakdown phenomenon occurs in the ordinary T-junction flow when the Reynolds number exceeds a critical value and is responsible for the trapped bubbles as well as similar multiphase flow phenomenon in angled junctions [53]. Our interpretation of the detailed numerical simulations showed that above the critical Reynolds number the subcritical character of the flow set the recirculation that highlights the closed streamline region of vortex breakdown. Also, we reported the variation of the critical Reynolds number R_c with the angle of the junction α , and it is an open question whether there is a simple functional form, analogous to an effective Dean number, for the curve $R_c(\alpha)$. It seems that no one had previously observed or documented, in experiments or even single-phase flow simulations, these systematic changes with Reynolds number in these common flow configurations. I would like to think that these observations and ideas might be relevant in some practical situations.

V. CONCLUDING REMARKS

It is reasonable to ask what is the driving force for the different problems discussed in these pages. In my case I will admit to finding continual fascination with the kinds of questions, and applications, that arise in topics represented broadly in the multiphase and complex fluids areas. Talking with colleagues from all over the world is a continual source of education, joy, and surprises, as the topics in complex fluids touch so many disciplines. I suppose one might seek a unifying principle or set of principles (beyond the basic ideas of mechanics and fluid dynamics), but I can only find an enthusiastic approach for tackling, usually in collaboration, the problems in this area. I recognize that there can be underlying simple balances and scaling laws, sometimes already anticipated in classical problems available in the field, that perhaps can be identified with new experiments and models, and that asking good questions, which often happens in my case accidentally, is the key to moving forward.

HOWARD A. STONE

ACKNOWLEDGMENTS

Funding for some of the work discussed here was provided by the National Science Foundation, ONR (supported under ONR MURI Grants No. N00014-12-1-0875 and No. N00014-12-1-0962, Program Manager Dr. Ki-Han Kim), and Unilever Research. I am very grateful for this support. I thank W. M. Hamner for providing further information on the images of the phalarope shown in Fig. 1. I thank the many people whose work is discussed in this article, as the discussion above should make clear that I have benefited and learned from collaborations with many people.

-
- [1] M. D. van Dyke, *An Album of Fluid Motion* (Parabolic Press, Palo Alto, 1982).
- [2] M. Samimy, K. S. Breuer, L. G. Leal, and P. H. Steen (eds.), *A Gallery of Fluid Motion* (Cambridge University Press, Cambridge, 2003).
- [3] B. S. Obst, W. M. Hamner, P. P. Hamner, E. Wolanski, M. Rubega, and B. Littlehales, Kinematics of phalarope spinning, *Nature (London)* **384**, 121 (1996).
- [4] M. Prakash, D. Quéré, and J. W. M. Bush, Surface tension transport of prey by feeding shorebirds: The capillary ratchet, *Science* **320**, 931 (2008).
- [5] I. Cantat, S. Cohen-Addad, F. Elias, F. Graner, R. Höhler, O. Pitois, F. Rouyer, and A. Saint-Jalmes, *Foams: Structure and Dynamics* (Oxford University Press, Oxford, 2013).
- [6] J. L. Anderson, Colloid transport by interface forces, *Ann. Rev. Fluid Mech.* **21**, 61 (1989).
- [7] B. Abécassis, C. Cottin-Bizonne, C. Ybert, A. Ajdari, and L. Bocquet, Boosting migration of large particles by solute contrasts, *Nat. Mater.* **7**, 785 (2008).
- [8] D. Velegol, A. Garg, R. Guha, A. Kar, and M. Kumar, Origins of concentration gradients for diffusiophoresis, *Soft Matter* **12**, 4686 (2016).
- [9] S. Shin, O. Shardt, P. B. Warren, and H. A. Stone, Membraneless water filtration using CO₂, *Nat. Commun.* **8**, 15181 (2017).
- [10] D. Saintillan and M. J. Shelley, Theory of active suspensions, in *Complex Fluids in Biological Systems*, edited by S. Spagnolie (Springer Science+Business Media, New York, 2015), pp. 391–355.
- [11] S. J. Muller, R. G. Larson, and E. S. G. Shaqfeh, A purely elastic transition in Taylor-Couette flow, *Rheol. Acta* **28**, 499 (1989).
- [12] A. Groisman and V. Steinberg, *Nature (London)* **405**, 53 (2000).
- [13] A. Sauret, F. Boulogne, J. Cappello, E. Dressaire, and H. A. Stone, Damping of liquid sloshing by foams, *Phys. Fluids* **27**, 022103 (2015).
- [14] S. Shim and H. A. Stone, Damped coalescence cascade of liquid drops, *Phys. Rev. Fluids* **2**, 044001 (2017).
- [15] Y. E. Yu, S. Khodaparast, and H. A. Stone, Armoring confined bubbles in the flow of colloidal suspensions, *Soft Matter* **13**, 2857 (2017).
- [16] N. Oppenheimer, S. Navardi, and H. A. Stone, Motion of a hot particle in viscous fluids, *Phys. Rev. Fluids* **1**, 014001 (2016).
- [17] L. E. Stillwagon and R. G. Larson, Fundamentals of topographic substrate leveling, *J. Appl. Phys.* **63**, 5251 (1988).
- [18] S. Kalliadasis, C. Bielarz, and G. M. Homsy, Steady free-surface thin film flows over topography, *Phys. Fluids* **12**, 1889 (2000).
- [19] E. Dressaire, L. Courbin, J. Crest, and H. A. Stone, Thin-Film Fluid Flows Over Micro Decorated Surfaces: Observation of Polygonal Hydraulic Jumps, *Phys. Rev. Lett.* **102**, 194503 (2009).
- [20] E. Dressaire, L. Courbin, J. Crest, and H. A. Stone, Inertia dominated thin-film flows over micro decorated surfaces, *Phys. Fluids* **22**, 073602 (2010).
- [21] M. Joanicot and A. Ajdari, Droplet control for microfluidics, *Science* **309**, 887 (2005).
- [22] J. K. Nunes, S. S. H. Tsai, J. Wan, and H. A. Stone, Dripping and jetting in microfluidic multiphase flows applied to particle and fibre synthesis, *J. Phys. D: Appl. Phys.* **46**, 114002 (2013).

SEEKING SIMPLICITY FOR THE UNDERSTANDING OF . . .

- [23] P. G. Saffman and G. I. Taylor, The penetration of a fluid into a porous medium or Hele-Shaw cell containing a more viscous liquid, *Proc. R. Soc. London A* **245**, 312 (1958).
- [24] S. Hill, Channelling in packed columns, *Chem. Eng. Sci.* **1**, 247 (1952).
- [25] R. L. Chouke, P. van Meurs, and C. van der Poel, The instability of slow, immiscible, viscous liquid-liquid displacements in permeable media, *Trans. AIME* **216**, 188 (1959).
- [26] G. M. Homsy, Viscous fingering in porous media, *Ann. Rev. Fluid Mech.* **19**, 271 (1987).
- [27] S. Protière, M. Z. Bazant, D. A. Weitz, and H. A. Stone, Droplet breakup in flow past an obstacle: A capillary instability due to permeability variations, *Europhys. Lett.* **92**, 54002 (2010).
- [28] J. R. A. Pearson, The instability of uniform viscous flow under rollers and spreaders, *J. Fluid Mech.* **7**, 481 (1960).
- [29] E. Pitts and J. Greiller, The flow of thin liquid films between rollers, *J. Fluid Mech.* **11**, 33 (1961).
- [30] K. J. Ruschak, Coating flows, *Annu. Rev. Fluid Mech.* **17**, 65 (1985).
- [31] M. Rabaud, S. Michalland, and Y. Couder, Dynamical Regimes of Directional Viscous Fingering: Spatiotemporal Chaos and Wave Propagation, *Phys. Rev. Lett.* **64**, 184 (1990).
- [32] D. A. Reinelt, The primary and inverse instabilities of directional viscous fingering, *J. Fluid Mech.* **285**, 303 (1995).
- [33] T. T. Al-Housseiny, P. A. Tsai, and H. A. Stone, Control of interfacial instabilities using flow geometry, *Nat. Phys.* **8**, 747 (2012).
- [34] D. Pihler-Puzović, P. Illien, M. Heil, and A. Juel, Suppression of Complex Fingerlike Patterns at the Interface Between Air and a Viscous Fluid by Elastic Membranes, *Phys. Rev. Lett.* **108**, 074502 (2012).
- [35] G. G. Peng, D. Pihler-Puzović, A. Juel, M. Heil, and J. R. Lister, Displacement flows under elastic membranes. Part 2. Analysis of interfacial effects, *J. Fluid Mech.* **784**, 512 (2015).
- [36] D. Quéré, Non-sticking drops, *Rep. Prog. Phys.* **68**, 2495 (2005).
- [37] D. Angelescu, T. Moscato, F. Pauchet, and R. Van Kuijk, U.S. Patent No. 0283778 (2011).
- [38] T.-S. Wong, S. H. Kang, S. K. Tang, E. J. Smythe, B. D. Hatton, A. Grinthal, and J. Aizenberg, Bioinspired self-repairing slippery surfaces with pressure-stable omniphobicity, *Nature (London)* **477**, 443 (2011).
- [39] A. Lafuma and D. Quéré, Slippery pre-suffused surfaces, *Europhys. Lett.* **96**, 56001 (2011).
- [40] E. Lauga and H. A. Stone, Effective slip in pressure-driven Stokes flow, *J. Fluid Mech.* **489**, 55 (2003).
- [41] C. Cottin-Bizonne, J. L. Barrat, L. Bocquet, and E. Charlaix, Low-friction flows of liquid at nanopatterned interfaces, *Nat. Mater.* **2**, 237 (2003).
- [42] J. R. Philip, Flows satisfying mixed no-slip and no-shear conditions, *Z. Angew. Math. Phys.* **23**, 353 (1972a).
- [43] J. R. Philip, Integral properties of flows satisfying mixed no-slip and no-shear conditions, *Z. Angew. Math. Phys.* **23**, 960 (1972b).
- [44] J. S. Wexler, I. Jacobi, and H. A. Stone, Shear-Driven Failure of Liquid-Infused Surfaces, *Phys. Rev. Lett.* **114**, 168301 (2015).
- [45] Y. Liu, J. S. Wexler, C. Schönecker, and H. A. Stone, Effect of viscosity ratio on the shear-driven failure of liquid-infused surfaces, *Phys. Rev. Fluids* **1**, 074003 (2016).
- [46] D. Vigolo, S. Radl, and H. A. Stone, Unexpected trapping of particles at a T junction, *Proc. Nat. Acad. Sci. USA* **111**, 4770 (2014).
- [47] K. K. Chen, C. W. Rowley, and H. A. Stone, Vortex dynamics in a pipe T-junction: Recirculation and sensitivity, *Phys. Fluids* **27**, 034107 (2015).
- [48] W. R. Dean, Note on the motion of fluid in a curved pipe, *Phil. Mag.* **4**, 208 (1927).
- [49] G. L. Brown and J. M. Lopez, Axisymmetric vortex breakdown Part 2. Physical mechanisms, *J. Fluid Mech.* **221**, 553 (1990).
- [50] H. Squire, *Analysis of the Vortex Breakdown Phenomenon* (Imperial College of Science and Technology, Aeronautics Department, London, 1960).
- [51] T. B. Benjamin, Theory of the vortex breakdown phenomenon, *J. Fluid Mech.* **14**, 593 (1962).
- [52] S. Wang and Z. Rusak, The dynamics of a swirling flow in a pipe and transition to axisymmetric vortex breakdown, *J. Fluid Mech.* **340**, 177 (1997).
- [53] J. T. Ault, A. Fani, K. K. Chen, S. Shin, F. Gallaire, and H. A. Stone, Vortex-Breakdown-Induced Particle Capture in Branching Junctions, *Phys. Rev. Lett.* **117**, 084501 (2016).